Paul Richards,[1] Helen E. Parker,[1] Alice E. Adriaenssens,[1] Joshua M. Hodgson,[1] Simon C. Cork,[2] Stefan Trapp,[2] Fiona M. Gribble,[1] and Frank Reimann[1]

Identification and Characterization of GLP-1 Receptor–Expressing Cells Using a New Transgenic Mouse Model

GLP-1 is an intestinal hormone with widespread actions on metabolism. Therapies based on GLP-1 are highly effective because they increase glucose-dependent insulin secretion in people with type 2 diabetes, but many reports suggest that GLP-1 has additional beneficial or, in some cases, potentially dangerous actions on other tissues, including the heart, vasculature, exocrine pancreas, liver, and central nervous system. Identifying which tissues express the GLP-1 receptor (GLP1R) is critical for the development of GLP-1–based therapies. Our objective was to use a method independent of GLP1R antibodies to identify and characterize the targets of GLP-1 in mice. Using newly generated glp1r-Cre mice crossed with fluorescent reporter strains, we show that major sites of *glp1r* expression include pancreatic β- and δ-cells, vascular smooth muscle, cardiac atrium, gastric antrum/pylorus, enteric neurones, and vagal and dorsal root ganglia. In the central nervous system, glp1r-fluorescent cells were abundant in the area postrema, arcuate nucleus, paraventricular nucleus, and ventromedial hypothalamus. Sporadic glp1r-fluorescent cells were found in pancreatic ducts. No glp1r-fluorescence was observed in ventricular cardiomyocytes. Enteric and vagal neurons positive for glp1r were activated by GLP-1 and may contribute to intestinal and central responses to locally released GLP-1, such as regulation of intestinal secretomotor activity and appetite.

Diabetes 2014;63:1224–1233 | DOI: 10.2337/db13-1440

GLP-1 is one of several metabolically active peptides that are released from enteroendocrine cells in the gut epithelium after food intake. Together with glucose-dependent insulinotropic polypeptide (GIP), GLP-1 accounts for up to 70% of meal-stimulated insulin secretion in a phenomenon known as the incretin effect. Therapies based on GLP-1 were developed originally on the basis that they enhance insulin secretion in people with type 2 diabetes, but are now known also to lower glucagon levels, slow gastric emptying, and reduce appetite (1). More surprising are reports that GLP-1 improves memory and learning (2), is cardioprotective during myocardial ischemia (3), promotes hepatocyte function (4), and increases pancreatic exocrine

[1]Cambridge Institute for Medical Research and Medical Research Council Metabolic Diseases Unit, Addenbrooke's Hospital, Cambridge, U.K.
[2]Department of Neuroscience, Physiology and Pharmacology, University College London, London, U.K.
Corresponding author: Fiona M. Gribble, fmg23@cam.ac.uk.

Received 19 September 2013 and accepted 21 November 2013.

This article contains Supplementary Data online at http://diabetes.diabetesjournals.org/lookup/suppl/doi:10.2337/db13-1440/-/DC1.

P.R. and H.E.P. are joint first authors. F.M.G. and F.R. are joint senior authors.

See accompanying article, p. 1182.

hyperplasia (5). A critical obstacle to distinguishing direct from indirect effects of GLP-1, however, is our incomplete understanding of which cell types express receptors for GLP-1 (6).

The GLP-1 receptor (GLP1R) was cloned originally from pancreatic β-cells, where it is coupled to cyclic adenosine monophosphate (cAMP) production and enhanced glucose-dependent insulin release (7). GLP1R is a high-affinity receptor for "active" GLP-1, a term encompassing GLP-1(7-36)amide and GLP-1(7-37) that are released postprandially from enteroendocrine L-cells in the epithelium of the small and large intestine (8). Although believed to target β-cells through the bloodstream, GLP-1 is rapidly cleaved and inactivated by dipeptidyl peptidase 4 (DPP4) (9) once it enters the circulation. This has led to the idea that receptors located close to L-cells may act as local sensors of endogenous GLP-1 before it is inactivated. One proposed signaling route involves GLP1R located on branches of the afferent vagus nerve innervating the portal vein (10). Some reports suggest that DPP4-cleaved GLP-1 may also be a weak partial agonist or antagonist of GLP1R (11), eliciting physiological responses such as vasodilation (12). Elucidating the actions of GLP-1 and its metabolites is critical for our understanding of postprandial physiology and the pharmacology of clinically approved GLP-1 mimetics and DPP4 inhibitors.

Identifying which tissues and cell types express GLP1R faces the obstacle that many existing antibodies to GLP1R lack specificity (6). The objective of this study was to identify and characterize targets of GLP-1 by a method independent of the use of antibodies and to investigate whether *glp1r* is expressed in cells located close to enteroendocrine cells. For this purpose, we generated a transgenic mouse model in which the *glp1r* promoter drives Cre recombinase. By cloning Cre into the coding sequence of *glp1r* in a bacterial artificial chromosome (BAC), we aimed to retain the receptor promoter, together with long 5′ and 3′ sequences, and achieve cell-specific expression mirroring that of native *glp1r*. When crossbred with floxed reporter strains, these mice produce offspring expressing fluorescent markers in target tissues that currently, or during development, express *glp1r*.

RESEARCH DESIGN AND METHODS

Animals

Animal procedures were approved by the local ethics committee and conformed to United Kingdom Home Office regulations. Mice were killed by cervical dislocation, and the various tissue types were collected into ice-cold Leibovitz-15 (L-15) medium (unless otherwise stated, all chemicals were supplied by Sigma-Aldrich, Poole, U.K.). Ganglia were collected directly into 4% paraformaldehyde for immunohistochemistry.

Generation of Mice

To express Cre recombinase under the control of the *glp1r* promoter, we replaced the sequence between the start codon in exon 1 and the stop codon in exon 13 in the murine-based BAC RP23-408N20 (Children's Hospital Oakland Research Institute, Oakland, CA) initially by a counter-selection cassette rpsL-neo (Gene Bridges, Heidelberg, Germany) and subsequently by the improved Cre (iCre) sequence (13) using Red/ET recombination technology (Gene Bridges) (Fig. 1*A*). Briefly, the rpsL-neo or iCre sequences were amplified by PCR adding *glp1r*-gene specific 3′ and 5′ sequences (see oligonucleotides in Supplementary Table 1), and homologous recombination was achieved upon cotransforming the BAC containing *Escherichia coli* DH10B clone with the PCR product and the plasmid pSC101-BAD-gbaA, which provides the recombination enzymes (Gene Bridges). Positive recombinants were isolated using appropriate antibiotic selection and characterized by PCR and restriction analysis. Identity and correct positioning of the introduced iCre sequence was confirmed by direct sequencing using the oligonucleotides in Supplementary Table 1. BAC DNA for microinjection was purified using the large-construct Maxi-Prep kit (Qiagen, Manchester, U.K.) and dissolved at ~1–2 ng/μL in injection buffer containing (mmol/L): 10 Tris-HCl (pH 7.5), 0.1 EDTA, 100 NaCl, 0.03 spermine, and 0.07 spermidine. Pronuclear injection into ova derived from C57B6/CBA F1 parents and reimplantation of embryos into pseudopregnant females was performed by the Central Biomedical Services at Cambridge University. DNA of pups was isolated from ear clips by proteinase K digestion and screened for the transgene by PCR using the following primer pairs (Supplementary Table 1): GLP1R-001/Cre001 (462 bp) and Cre002/003 (537 bp) duplexed with RM41/42 (220 bp), which amplifies a β-catenin sequence used as a DNA quality control. The founder strain was backcrossed for more than eight generations onto a C57B6 background. The Cre-reporter transgenes used in the study, Rosa26–tandem-dimer red fluorescent protein (tdRFP) or –enhanced yellow fluorescent protein (EYFP), also on a C57B6 background, were screened for with the PCR primers tdRFP sense/anti (726 bp) and green fluorescent protein (GFP)002/003 (470 bp), respectively.

Flow Cytometry

Pancreatic islets were isolated and dispersed as described previously (8). Cell suspensions were separated by fluorescence-assisted cell sorting (FACS) using a MoFlo Beckman Coulter Cytomation sorter (Beckman Coulter, Inc., Hialeah, FL) or analyzed using a BD LSRFortessa analyzer (BD Biosciences, San Jose, CA). Side scatter (SSC), forward scatter, and pulse-width gates were used to exclude debris and aggregates. Islet populations were sorted into RNAse-free collection buffer for mRNA analysis, or into protein lysis buffer (50 mmol/L Tris-HCl, 150 mmol/L NaCl, 1% IGEPAL-CA 630, 0.5%

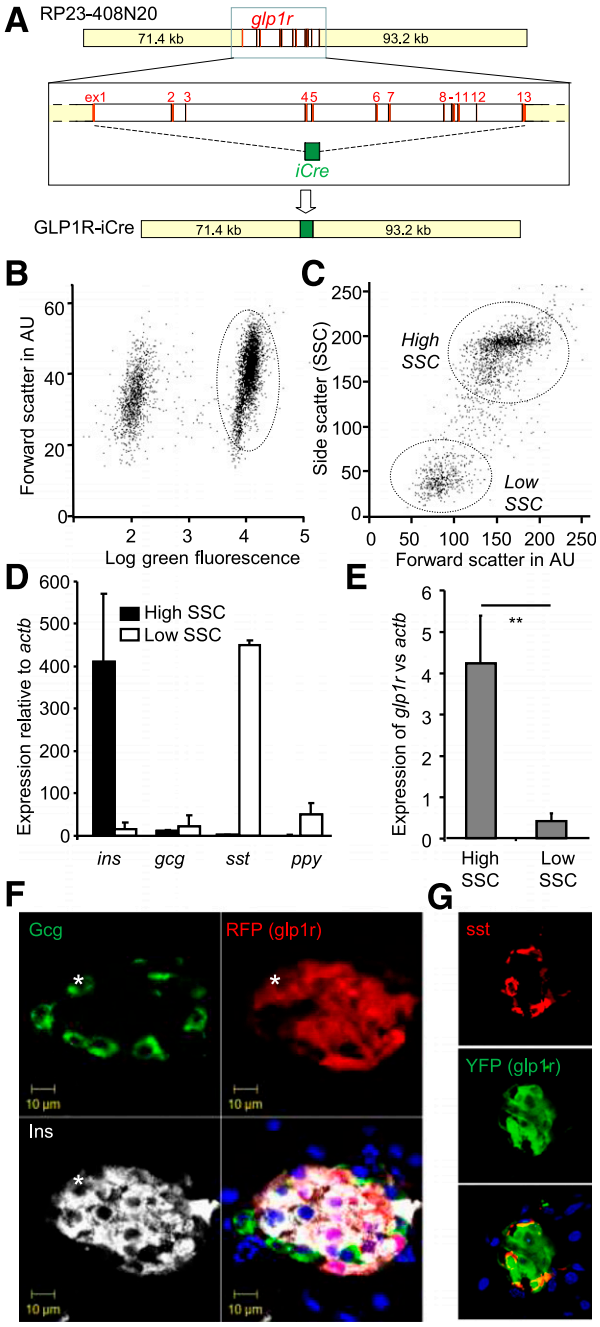

Figure 1—Glp1r-Cre transgenic mice labeled pancreatic β- and δ-cells. *A*: Schematic depicts the insert of the BAC RP23-408N20 and replacement of the *glp1r* coding region from exons (ex) 1–13 with *iCre*. Lengths (in kb) of the murine genomic sequence 3′ and 5′ of the *glp1r* coding region in the BAC are indicated. *B*: Dispersed pancreatic islet cells from glp1r-Cre/ROSA26-YFP mice, analyzed by FACS. Green (yellow) fluorescence was measured by excitation at 488 nm and emission at 530/20 nm and is plotted against forward scatter in arbitrary units (AU). *C*: Cells with high red fluorescence from glp1r-Cre/ROSA26-tdRFP mice were FACS separated into populations with low and high SSC. These were analyzed by qRT-PCR for expression of hormones (*D*) or *glp1r* (*E*). $n = 3$ each; $^{**}P < 0.01$ by Student *t* test. Fixed pancreatic slices were coimmunostained RFP or YFP (representing glp1r fluorescence) together with glucagon and insulin (*indicates a cell triple-positive for glucagon, insulin, and glp1r fluorescence) (*F*) or somatostatin (*G*). Nuclei are visualized with Hoechst stain.

deoxycholic acid, and 1 tablet of complete EDTA-free protease inhibitor cocktail [Roche]) for measurement of GLP-1 content by MSD total and active GLP-1 assays (Mesoscale Discovery, Rockville, MD). FACS-analyzed samples were processed using FlowJo 7.6 software.

Quantitative RT-PCR

RNA from homogenized tissues was extracted using TRI Reagent or the RNeasy Micro Kit (Qiagen). RNA was treated with DNAse I (Ambion), and reverse transcribed according to standard protocols. Quantitative (q)RT-PCR was performed as described previously (8) using primers/probes as indicated in Supplementary Table 1. Expression of the test gene was measured relative to that of *actb* measured in parallel in the same sample using the ΔCt method. Data are presented as $2^{\Delta Ct}$, with the upper SEM calculated from the SEM of the ΔCt data.

Immunohistochemistry

Tissues were fixed in 4% paraformaldehyde, dehydrated in 15% and 30% sucrose, and frozen in optimal cutting temperature embedding media (CellPath, Newtown, U.K.). Cryostat-cut sections (6–10 µm) were mounted directly onto polylysine-covered glass slides (VWR, Leuven, Belgium). Slides were incubated for 1 h in blocking solution containing 10% goat or donkey serum and overnight in PBS/0.05% Triton X-100/10% serum with primary antisera of interest (Supplementary Table 1). Sections were washed with PBS and incubated with appropriate secondary antisera (donkey or goat AlexaFluors 488, 546, 555 or 633; Invitrogen) diluted 1:300. Control sections were stained with secondary antisera alone. Sections were mounted with Prolong Gold (Life Technologies) before confocal microscopy (Zeiss LSM 510, Carl Zeiss, Cambridge, U.K.).

Immunofluorescence of Brain Sections

Mice under ketamine and medetomidine anesthesia were perfused transcardially with 4% formaldehyde in PBS (pH 7.4). Brains were removed, postfixed overnight in the same fixative, and cryoprotected in 30% sucrose. Coronal sections were cut to 30 µm using a cryostat and washed in 0.1 mol/L phosphate buffer (PB; pH 7.4). After incubation in blocking buffer containing 10% sheep serum and 0.1% Triton X-100 diluted in 0.1 mol/L PB for 30 min at room temperature, sections were transferred to 1:1000 anti-DsRed (Clontech #632496) in blocking buffer and incubated overnight on a shaker at 4°C. Sections were washed three times in PB and incubated with 1:500 Cy3-conjugated anti-rabbit secondary antibody (Sigma-Aldrich #C2306) in blocking buffer for 2 h on a shaker at room temperature. Sections were washed in PB, mounted onto slides, and air dried before being coverslipped and viewed using epifluorescence (Eclipse 80; Nikon, Kingston upon Thames, U.K.). Photomicrographs were taken with a Micropublisher 3.3 RTV camera

and QCapture Pro software (QImaging, Inc., Surrey, BC, Canada).

Nodose and Enteric Ganglia Culture

Nodose ganglia (NG) were transferred into Dulbecco's modified Eagle's medium (DMEM) containing 1 mg/mL collagenase type 1 and trypsin (Worthington Biochemical Corp., Lakewood, NJ). For enteric ganglia culture, the small intestinal muscle layer was minced and digested in DMEM containing 1.5 mg/mL collagenase I and 1.3 mg/mL trypsin. All ganglia were digested for 1 h at 37°C and dissociated by trituration. Cells were plated on polylysine-coated dishes, and after attachment, dishes were flooded with DMEM supplemented with 10% (v/v) FBS, 100 units/mL penicillin, 0.1 mg/mL streptomycin, and 50 ng/mL nerve growth factor. Calcium imaging and electrophysiology were performed within 48 h of dissociation.

Calcium Imaging

NG cultures were loaded in 2 μmol/L Fura-2-acetoxymethyl ester (Invitrogen, Life Technologies, Paisley, U.K.) for 30 min in standard saline solution containing (mmol/L) 4.5 KCl, 138 NaCl, 4.2 $NaHCO_3$, 1.2 NaH_2PO_4, 2.6 $CaCl_2$, 1.2 $MgCl_2$, 5 glucose, and 10 HEPES (pH 7.4, NaOH). Imaging was performed as described previously (8). Fura2 was excited at 340 and 380 nm and RFP at 555 nm. Fura2 fluorescence measurements were taken every 3 s, and the background was corrected and expressed as the 340-to–380-nm ratio. Average fluorescence ratios were determined over 20 s, and responses were expressed as the maximum ratio achieved during stimulation divided by the mean of the ratios measured before and after washout. Cells were included in the analysis if they responded to 30 mmol/L KCl.

Nested PCR

After digestion and trituration, small enteric ganglia were picked using a glass capillary pipette filled with RNAse-free PBS. The pipette tip was crushed into RNAse-free collection buffer (4 μL First Strand Buffer [Invitrogen, U.K.], 4 μL RNAse-free water, and 1 μL RNAseOUT). Samples were reverse-transcribed using SuperScript III (Invitrogen, U.K.) using standard protocols. *Actb* and *glp1r* were amplified by multiplex nested PCR using 25 cycles each and the primers given in Supplementary Table 1.

Electrophysiology

Experiments were performed on identified RFP-positive cells in 12- to 48-h-old cultures containing partially dissociated enteric ganglia from glp1r-Cre/ROSA26-tdRFP mice. Microelectrodes were pulled from borosilicate glass (GC150 TF-15; Harvard Apparatus, Kent, U.K.) and the tips coated with refined yellow beeswax. Pipette solution contained (mmol/L) 107 KCl, 1 $CaCl_2$, 7 $MgCl_2$, 11 EGTA, 10 HEPES, and 5 K_2ATP (pH 7.2 KOH). Membrane potential was recorded using a Axopatch 200B and pCLAMP software (Molecular Devices, Berkshire, U.K.) in the standard whole-cell patch configuration at room temperature. Cells were perfused with standard saline solution (see above), to which GLP-1 was added as indicated.

Data Analysis

Data are presented as mean ± SEM. Statistical analysis was performed using Microsoft Excel and GraphPad Prism 5.0 software. Data that were normally distributed were analyzed by Student *t* test or ANOVA with post hoc Bonferroni test, as indicated in the figure legends. Calcium imaging and electrophysiology data were analyzed with the nonparametric tests, Mann-Whitney, or Wilcoxon rank sign test, as indicated, with a threshold for significance of $P < 0.05$.

RESULTS

Two glp1r-Cre founder strains containing the transgenic constructs depicted in Fig. 1*A* were generated and crossed with a ROSA26-tdRFP reporter (14). Tissues/cells in which the fluorescent reporter is visible directly or by immunostaining are described here as exhibiting glp1r fluorescence. One founder strain showed sparse glp1r fluorescence in pancreatic islets and was discontinued. The other showed marked islet fluorescence consistent with the known expression of *glp1r* in β-cells and was used for all analyses. It was crossed with a ROSA26-YFP reporter strain to generate mice producing YFP in *glp1r*-expressing cells and with GLU-Venus (8) to enable the colabeling of pancreatic α-cells and enteroendocrine L-cells that make glucagon/GLP-1.

Glp1r in the Pancreas

FACS analysis of pancreatic islet cell suspensions revealed a glp1r-fluorescent population (Fig. 1*B*) that could be divided into two groups with distinct SSC (Fig. 1*C*). These were separated by FACS, analyzed for expression of *ins*, *gcg*, *sst*, and *ppy* by qRT-PCR, and found to correspond to β-cells (high SSC) and δ-cells (low SSC) (Fig. 1*D*). Expression of *glp1r* in both populations was confirmed by qRT-PCR (Fig. 1*E*) and was ~10-fold lower in δ-cells than in β-cells ($P = 0.006$). Colocalization of glp1r fluorescence with insulin or somatostatin immunostaining was also evident in pancreatic slices (Fig. 1*F* and *G*).

To investigate expression of *glp1r* in α-cells, we examined pancreata from glp1r-Cre/ROSA26-tdRFP/GLU-Venus mice, in which α-cells are additionally labeled with Venus. By FACS analysis, only 9.5 ± 1.4% of α-cells ($n = 11$) were glp1r-fluorescent, consistent with the low expression of *glp1r* in the total α-cell population (Fig. 2*A*) and our previous detection of GLP1R immunofluorescence in a small proportion of α-cells (15). The population of α-cells exhibiting glp1r fluorescence was found by qRT-PCR to express *gcg*, as predicted, but also had significantly more *ins* than their non–glp1r-fluorescent α-cell counterparts (Fig. 2*B*). Rare cells immunopositive for insulin, glucagon, and glp1r-RFP were correspondingly identified in tissue slices (see cell marked with

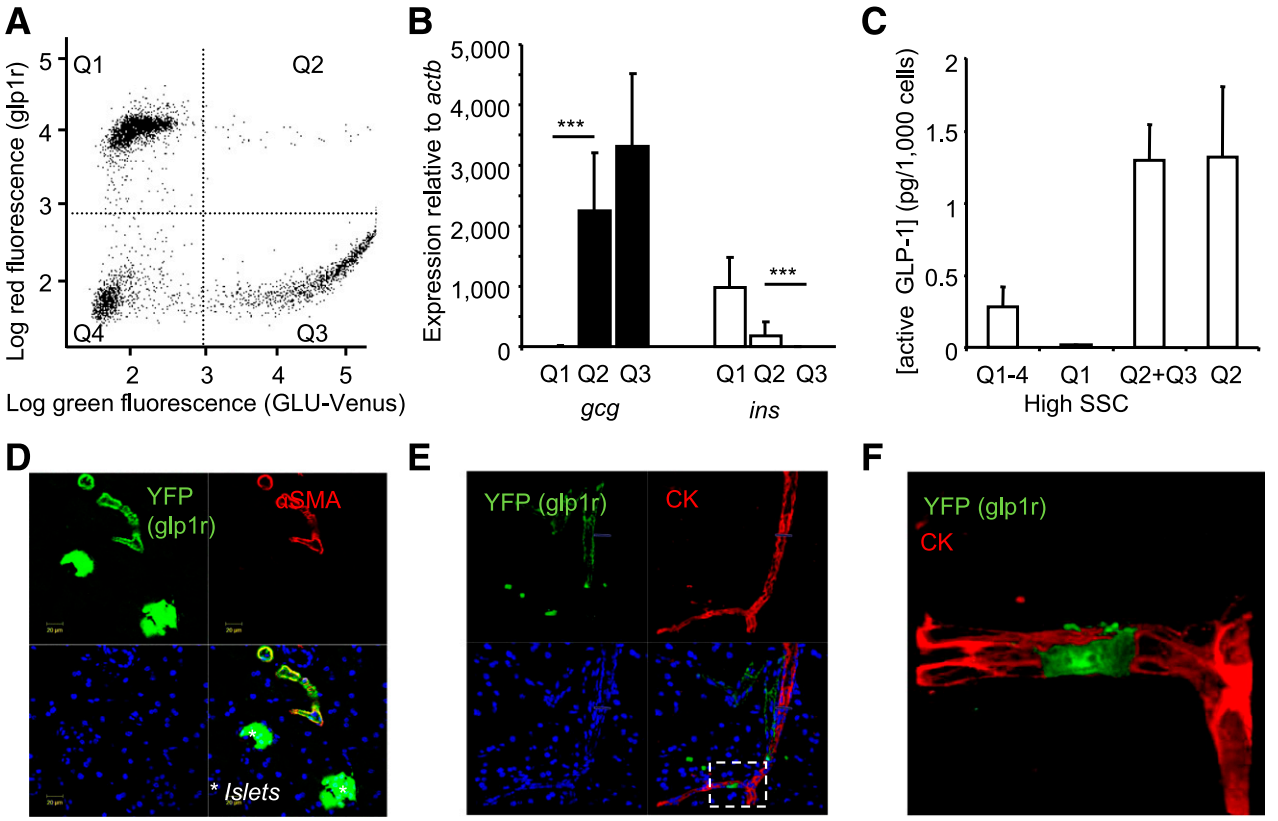

Figure 2— Glp1r in pancreatic α-cells. *A*: Islet cells from glp1r-Cre/ROSA26-tdRFP/GLU-Venus mice, analyzed by FACS to show red fluorescence (representing expression of *glp1r*) or green fluorescence (representing expression of *gcg*). *B*: Single- or double-positive cells were purified from Q1–Q3 marked in *A*, and analyzed for expression of *ins* and *gcg* by qRT-PCR. ***$P < 0.001$ by ANOVA with post hoc Bonferroni test, $n = 5–7$. *C*: Active GLP-1 hormone concentrations in cells collected from different quadrants of *A* as indicated. Q1–4 all islet cells, Q1 + high SSC β-cells, Q2 + Q3 all α-cells, and Q2 double-fluorescent cells (mean and SEM of four FACS sorts, each of pooled islets from one to two mice). *D–F*: Pancreatic sections from glp1r-Cre/ROSA26-YFP mice coimmunostained for α-SMA or cytokeratin (CK) together with YFP. The marked area in *E* is shown at higher magnification in *F*. Q, quadrant.

asterisk in Fig. 1*F*). However, single- and double-fluorescent α-cells both contained very little active GLP-1 (Fig. 2*C*): ~1.5 pg/1,000 α-cells compared with ~650 pg/1,000 colonic L-cells (8).

In pancreatic slices, glp1r fluorescence was also evident in nonislet structures. Predominant labeling was observed in blood vessels, as similarly observed in other tissues (Fig. 2*D* and Fig. 3). Costaining with an antibody against cytokeratin revealed a few scattered glp1r-fluorescent cells in pancreatic ducts (Fig. 2*E* and *F*).

Glp1r in the Cardiovascular System

Prominent glp1r-fluorescent labeling was observed in the aorta (Fig. 3*A*) and in arteries and arterioles in a range of tissues, including the heart, kidney, pancreas, and intestine (Fig. 3). *Glp1r* mRNA was correspondingly detected in aorta by qRT-PCR (Fig. 3*B*). In the kidney (Fig. 3*C*), glp1r fluorescence was found in arterioles and colocalized with smooth muscle α-actin (α-SMA) and the pericyte marker NG2, suggesting the labeling of smooth muscle cells. Overlap of glp1r fluorescence with immunostaining for renin was also observed. In the intestine, many small blood vessels were glp1r-fluorescent and exhibited colocalization with α-SMA and NG2 (Fig. 3*D* and *E*). In tissue preparations where small veins could be seen lying adjacent to arterioles, glp1r fluorescence appeared restricted to the arterial circulation (Fig. 3*F*).

Ventricular myocardium was devoid of glp1r fluorescence, with the exception of vascular structures immunopositive for α-SMA (Fig. 3*G*). In line with a recent report (16) that GLP-1 stimulates secretion of atrial natriuretic factor, scattered glp1r-fluorescent cells were found throughout the atrial myocardium (Fig. 3*H*). Expression of *glp1r* mRNA mirrored these findings, being approximately sixfold higher in atrial than ventricular extracts (Fig. 3*B*).

Glp1r in the Central Nervous System and Afferent Neuronal Ganglia

Sections through the hypothalamus and brainstem of glp1r-Cre/ROSA26-tdRFP mice revealed RFP-positive cells in the area postrema, arcuate nucleus, ventromedial hypothalamus, and paraventricular nucleus (Fig. 4*A*), consistent with previous reports (17). Glp1r-fluorescent cell bodies and *glp1r* mRNA were found in ganglia of the

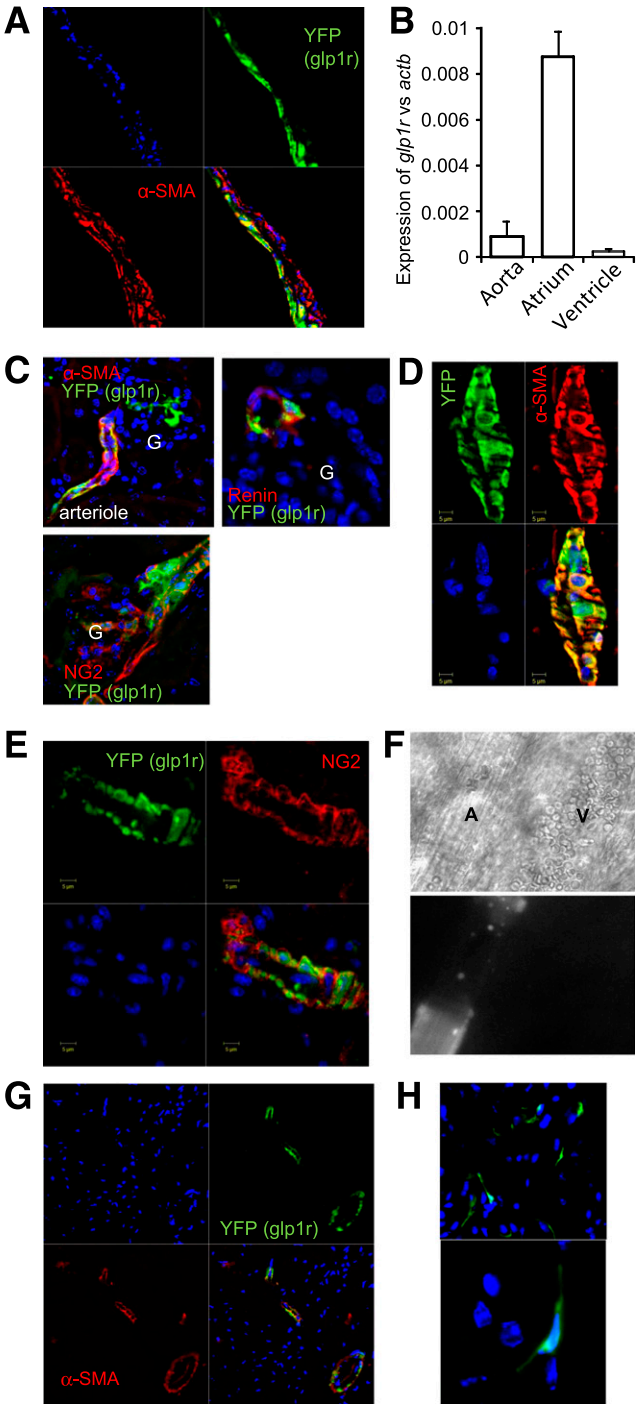

Figure 3—Glp1r in the cardiovascular system. Sections of aorta (*A*), kidney (*C*), intestine (*D* and *E*), and cardiac ventricle (*G*) or atrium (*H*) from glp1r-Cre/ROSA26-YFP mice were coimmunostained for YFP (representing glp1r fluorescence) and α-SMA, NG2, or renin, as indicated. In kidney sections, G depicts the position of glomeruli. *B*: qRT-PCR analysis of *glp1r* expression in aorta, atrium, and ventricle (geometric mean + 1 SEM, n = 5–6 each). *F*: Blood vessels in intestine from a glp1r-Cre/ROSA26-tdRFP mouse: light microscopy (A, arteriole; V, venule) (*upper panel*), tdRFP fluorescence (*lower panel*).

afferent vagus nerve (NG) (Fig. 4*B*) and dorsal root ganglia (DRG) (Fig. 4*C*), although by qRT-PCR we detected less *glp1r* mRNA in DRG than in NG (Fig. 4*D*). Consistent with the previous detection of calcitonin gene–related peptide (CGRP) in extrinsic sensory neurons innervating the gastrointestinal tract, a small population of glp1r-fluorescent neurons in DRGs were immunopositive for CGRP by immunostaining (Fig. 4*C*). In primary NG cultures, GLP-1 did not directly elevate intracellular Ca^{2+} concentrations but enhanced Ca^{2+} responses to ATP in glp1r-fluorescent cells, without affecting ATP responses in nonfluorescent cells (Fig. 4*E* and *F*). Cholecystokinin, leptin, and serotonin, by contrast, triggered larger Ca^{2+} responses in nonfluorescent than in glp1r-fluorescent neurons (Fig. 4*G*).

Glp1r in the Liver and Intestines

Hepatocytes were not glp1r-fluorescent, but fluorescent fibers were observed in the wall of the portal vein near the liver hilus (Fig. 5*A*), consistent with previous reports (10). Dense networks of glp1r-fluorescent fibers were found in the muscular and submucosal layers of the stomach in the vicinity of gastric pylorus (Fig. 5*B* and *C*), in some places exhibiting colabeling with neuronal nitric oxide synthetase (nNOS). Scattered glp1r-fluorescent neuronal fibers and cell bodies were identified in the small intestine and colon, but contrary to a recent report (18), the epithelial layer was largely devoid of glp1r fluorescence. *Glp1r* mRNA was correspondingly detected by PCR in myenteric ganglia containing glp1r-fluorescent cells (Fig. 5*D*). Patch clamp recordings of small intestinal myenteric neurones in primary culture revealed that glp1r-fluorescent neurons were electrically active and that their action potential frequency was increased by GLP-1 (Fig. 5*E* and *F*). Two glp1r-fluorescent cell populations were distinguishable electrophysiologically by the action potential waveform (Fig. 5*G*): 14 of 22 (64%) of neurons were the synaptic (*S*) type and 8 (36%) were the after-hyperpolarizing (AH) type.

Immunostaining for nNOS, a marker largely restricted to inhibitory motor neurones, revealed that 143 of 227 (63%) of glp1r-fluorescent neurones in small intestinal cultures (Fig. 5*H*) and 10 of 54 (19%) in colonic cultures (Fig. 5*I*) were nNOS-positive. Most nNOS-positive cell bodies, however, were glp1r-negative (small intestine, 3,523 of 3,666 [96%]; colon, 163 of 173 [94%]).
A smaller proportion of glp1r-fluorescent cells in culture stained for calretinin (small intestine, 7 of 142 [5%]; colon, 10 of 24 [42%]; Fig. 5*G* and *H*), CGRP, or calbindin (not shown), markers typically associated with intrinsic primary afferent neurones. Glp1r-fluorescent fibers were observed in the mucosa, in some cases relatively close to L-cells (Fig. 5*J*).

DISCUSSION

Despite wide academic and commercial interest in the actions of GLP-1, attempts to identify the cellular targets

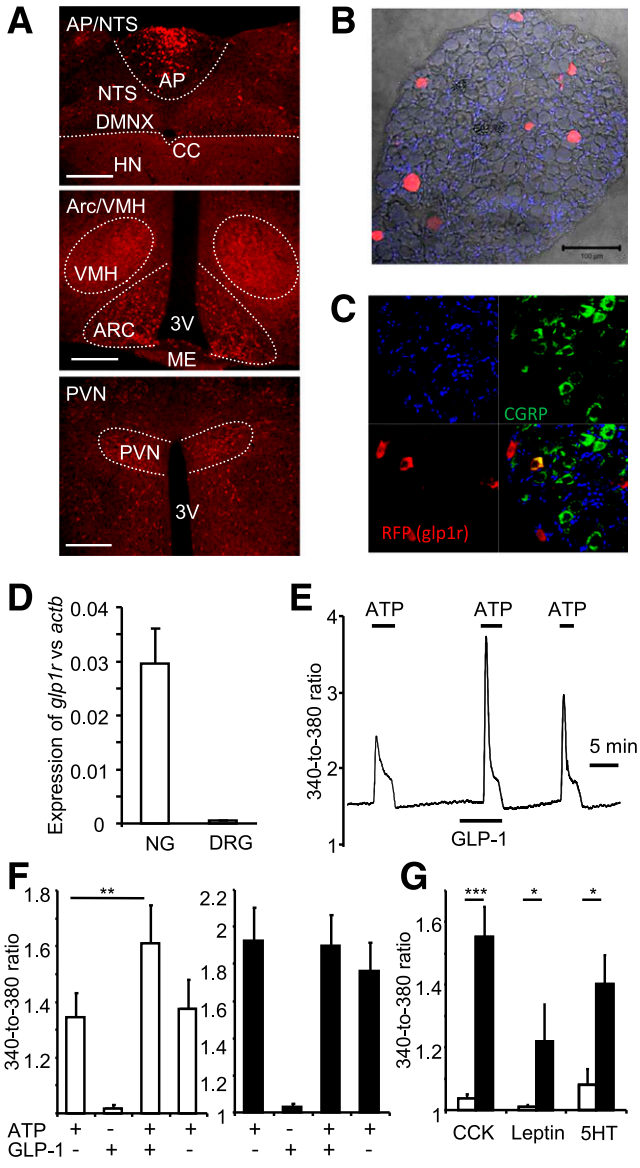

Figure 4—Glp1r in the brain and afferent neuronal ganglia. *A*: Coronal brain sections from glp1r-Cre/ROSA26-tdRFP mouse, immunostained for RFP. In caudal brainstem (*top*), a high density of fluorescent cells was observed in the area postrema (AP), whereas only few were evident in the nucleus of the solitary tract (NTS) and dorsal vagal nucleus (DMNX), and none were found in the hypoglossal nucleus (HN). In hypothalamus (*middle* and *lower panels*), large numbers of RFP fluorescent cells were observed in the arcuate nucleus (ARC), ventromedial hypothalamus (VMH), and paraventricular nucleus (PVN). 3V, 3rd ventricle; CC, central canal; ME, median eminence. Scale bar = 150 μm. *B*: Section of NG from glp1r-Cre/ROSA26-tdRFP mouse showing RFP-positive cells. *C*: DRG section from a glp1r-Cre/ROSA26-tdRFP mouse costained for RFP and CGRP. *D*: Whole NG or DRG were analyzed for *glp1r* vs. *actb* expression by qRT-PCR (geometric mean + 1 SEM of three each). *E*: NG from glp1r-Cre/ROSA26-tdRFP mice were studied by Fura2 Ca^{2+} imaging in primary culture. Representative trace from an RFP-positive NG neuron to ATP (0.5 μmol/L) applied in the absence or presence of GLP-1 (1 nmol/L), as indicated by the horizontal bars. *F*: Mean 340-to–380-nm fluorescence ratios from 13 RFP-positive cells (□) and 12 RFP-negative (■) cells, monitored as in *E* and normalized to baseline recorded in the absence of test agent. $^{**}P < 0.01$ by Wilcoxon signed rank test. *G*: Ca^{2+} responses of RFP-positive (□) and RFP-negative (■) cells to cholecystokinin (CCK) (10 nmol/L), leptin (10 nmol/L), or 5HT (10 μmol/L), normalized to baseline in control solution. From left to right, columns represent data from n = 18, 41, 9, 31, 14, and 35 cells, respectively. $^{*}P < 0.05$, $^{***}P < 0.001$ by Mann-Whitney test.

of GLP-1 are hampered by the lack of specificity of antibodies to GLP1R. Our development of a new transgenic mouse model expressing Cre recombinase driven by the *glp1r* promoter provides an antibody-independent method for the identification and characterization of live cells expressing *glp1r*, using floxed fluorescent reporter strains. The results illuminate not only which tissues exhibited glp1r fluorescence but also those that did not.

Establishing definitively that the GLP1R protein is produced by all glp1r-fluorescent cells will be important, because our use of Cre recombinase results in a permanent activation of the fluorescent reporters, even in cells that no longer express the receptor as well as in the progeny of cells that have once expressed *glp1r*. Where neurones were identified, we were able to confirm expression of GLP1R protein by demonstrating functional responsiveness to added GLP-1. In other cases, such as the kidney and heart, one would ideally demonstrate costaining of glp1r-fluorescent structures with antibodies against GLP1R, but this will remain difficult until better antibodies become available. It is possible that cells weakly expressing *glp1r* may generate insufficient Cre recombinase to activate the fluorescent reporters. This may explain our inability to confirm a recent report that GLP1R is located in the intestinal epithelial layer (18), but studies relying predominantly on the use of GLP1R antibodies should be interpreted with caution (6).

Throughout the body we observed glp1r fluorescence colocalizing with α-SMA in large and small arteries, suggesting that vascular smooth muscle is a potential target for circulating GLP-1. Consistent with these findings, chronic treatment with GLP-1 mimetics in patients with type 2 diabetes is associated with a small reduction in blood pressure and an increase in heart rate (19). The underlying physiology appears complex, however, and in rats, GLP-1 was found to act as a vasodilator in the periphery but as a vasoconstrictor in the splanchnic bed (20). Reports that DPP4-inactivated GLP-1 triggers vasodilation and that not all responses to GLP-1 are lost in mice lacking *glp1r* (12) have even led to the speculation that there may exist an alternative receptor responsive to GLP-1 and/or its metabolites. The vasodilatory effect of GLP-1 in mice was recently reported to be an indirect consequence of enhanced atrial natriuretic factor release (16). In support of this idea, we found that the cardiac atrium expressed particularly high levels of *glp1r* mRNA and had scattered glp1r-fluorescent cells in addition to the labeled vasculature. We also detected glp1r fluorescence in renal arterioles and in renin-producing cells, consistent with reports that GLP-1 has direct effects on the kidney (21).

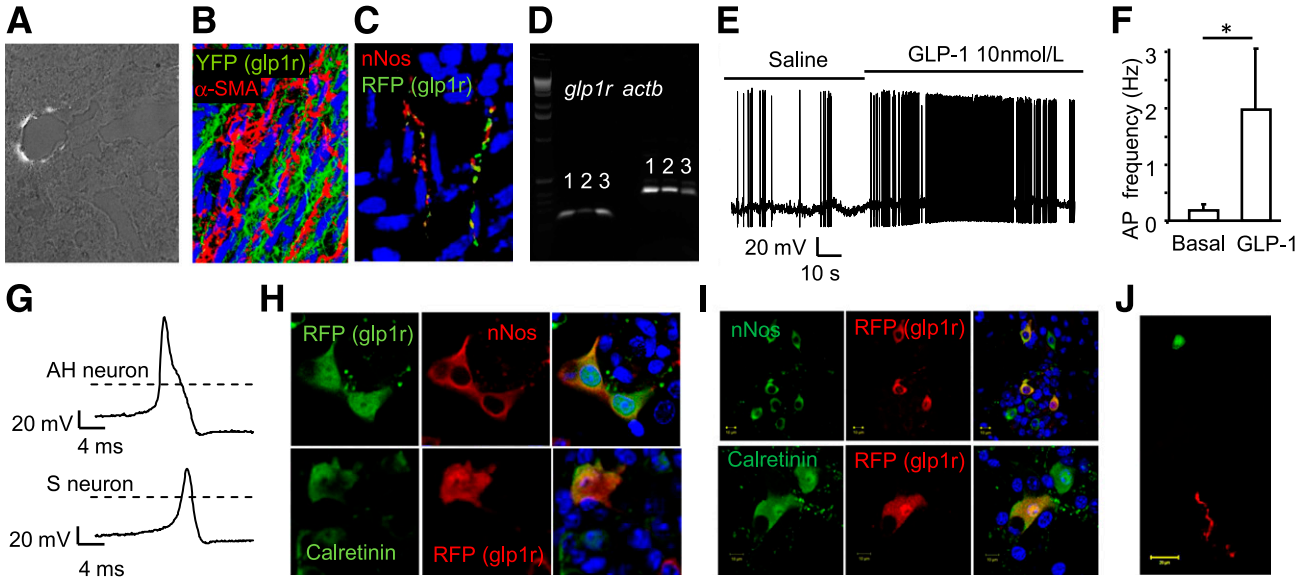

Figure 5—Glp1r in enteric neurons. *A*: Fixed-tissue section of liver from a glp1r-Cre/ROSA26-tdRFP mouse, showing glp1r fluorescence in structures surrounding a portal vein. Antral area of the stomach from a glp1r-Cre/ROSA26-tdRFP/ROSA26-YFP mouse, immunostained for YFP (green) and α-SMA (red) (*B*) and for RFP (green) and nNOS (red) (*C*). *D*: Nested PCR amplification of *glp1r* and *β-actin*, performed on three handpicked glp1r-fluorescent enteric ganglia from glp1r-Cre/ROSA26-tdRFP mice. *E*: Representative recording of a partially dissociated small intestinal glp1r-fluorescent enteric neuron in primary culture, monitored in whole-cell current clamp, after addition of GLP-1 (10 nmol/L). *F*: Mean action potential (AP) frequency of seven cells under basal conditions and after GLP-1 application. $^*P < 0.05$ by Wilcoxon signed rank test. *G*: Enteric neurons, recorded as in *E*, were divided into AH type (with characteristic hump on the action potential downstroke and AH) and S type. The dashed line represents the 0 mV line. Small intestinal (*H*) and colonic (*I*) tissue sections from a glp1r-Cre/ROSA26-tdRFP mouse costained for RFP together with nNOS or calretinin, as indicated. Because direct RFP fluorescence is lost on fixation, a green secondary antibody was used to visualize RFP in the *upper panels* of *H*. *J*: Intestinal tissue section from a glp1r-Cre/ROSA26-tdRFP/GLU-Venus mouse shows proximity of an L-cell (green) and a red glp1r-fluorescent fiber.

Despite literature suggesting direct cardioprotective effects of GLP-1, however, glp1r fluorescence was not observed in ventricular cardiomyocytes. In view of the prominent labeling of the arterial system, it seems likely that the reported effects of GLP-1 on cardiac function may be mediated indirectly via the coronary vasculature.

In pancreatic islets, *glp1r* expression was largely restricted to the β- and δ-cell populations, with only ~10% of α-cells exhibiting glp1r fluorescence. The finding that *glp1r* was expressed in δ-cells but was largely excluded from α-cells supports the idea that the inhibition of glucagon secretion by GLP-1 is mediated indirectly through enhanced somatostatin release (22). The role of the ~10% of α-cells that were glp1r-fluorescent but apparently expressed *ins* is unclear. Although we speculated that proglucagon may be alternatively processed in α-cells producing insulin, we found no evidence for production of substantial amounts of active GLP-1 in the double-fluorescent α-cell or the total α-cell population. In the exocrine pancreas, glp1r fluorescence was largely confined to the vasculature, with only sporadic glp1r-fluorescent cells identifiable in pancreatic ducts. Whether these sparse glp1r-positive α-cells and ductal cells are significant targets of GLP-1 mimetics will be of interest in the context of current concerns that incretin therapies may have adverse effects on the pancreas, triggering α-cell hyperplasia, pancreatitis, and pancreatic cancer (23).

In the brain stem, glp1r fluorescence was prominent in the area postrema. This is a region with a leaky blood–brain barrier that has been postulated previously as an area potentially capable of responding to circulating GLP-1 concentrations (24). In the hypothalamus, we found glp1r fluorescence in the arcuate and paraventricular nuclei, coinciding with the sites we found previously to receive projections from proglucagon-producing neurones in the nucleus of the tractus solitarius (25). These cells are therefore likely to form a component of the relay circuit linking the brainstem to the appetite-controlling networks of the hypothalamus.

The identification of glp1r-fluorescent neurons in the gastric antrum and pylorus, intestine, NG, and DRG may be relevant to understanding the local targets of intestinally released GLP-1. Dense innervation of the pylorus by glp1r-fluorescent fibers is consistent with the well-recognized action of GLP-1 to inhibit gastric emptying, the "ileal brake," although further studies will be required to elucidate the identity and origin of these fibers. Our functional analysis suggests that vagal cell bodies expressing *glp1r* form a distinct neuronal population, responding to GLP-1 but not cholecystokinin, leptin, or 5HT. That GLP-1 activates vagal afferent neurons terminating in the wall of the portal vein has been recognized for several years (10). Vagal innervation of the intestine, however, diminishes along the length of

the gastrointestinal tract and inversely mirrors the frequency of L-cells, which predominate in the distal gut. Our identification of glp1r-positive cell bodies in the enteric nervous system and DRGs suggests that GLP-1 may also signal to the central nervous system through local and spinal sensory nerves, potentially providing a signaling route recruited by GLP-1 released more distally. Whether the glp1r-fluorescent nerve fibers we observed in the intestinal mucosa, in some cases close to L-cells, represent the terminals of these "sensory" neurons or of enteric neurons remains to be elucidated.

Glp1r-fluorescent enteric neurons in primary culture exhibited increased firing frequency on application of GLP-1, but their functional role remains to be established. On the basis of the reported characteristics of guinea pig enteric neurones (26), our data suggest that the S-type neurons may correspond to the population of glp1r-fluorescent nNOS-positive cells and might thus play role in the local inhibition of circular and/or longitudinal muscle tone. The finding of AH-type electrophysiology in some cells and of coimmunostaining of glp1r fluorescence with calretinin, calbindin, and CGRP suggests that there is also a population of GLP-1-responsive intrinsic primary afferent neurones that may relay signals to other regions of the enteric nervous system or afferent neurons.

Glp1r-fluorescent afferent and enteric neuronal cell bodies and nerve fibers within the intestinal mucosa are of particular interest when considering the physiological consequences of food intake and bariatric surgery. Gastric bypass results in dramatically elevated GLP-1 levels, antagonism of which largely abolishes postsurgical improvements in glucose-stimulated insulin release (27). GLP-1 mimetics, however, are markedly less effective than surgery in treating type 2 diabetes. The physiological consequences of endogenous GLP-1, released locally at high levels after surgery and potentially reaching high concentrations at the site of local nerve endings, clearly deserve further attention. Current and future findings using our new mouse model promise to improve our understanding of the desirable and undesirable actions of this therapeutically fascinating hormone.

Acknowledgments. GLP-1 immunoassays were performed by Keith Burling at the Medical Research Council Metabolic Diseases Unit, Cambridge. The *iCre* was a kind gift from Rolf Sprengel, Heidelberg, Germany. Rosa26-tdRFP reporter mice were kindly provided by Hans Jörg Fehling, Ulm, Germany.

Funding. This research was funded by Wellcome Trust PhD studentships to P.R. and A.E.A., Wellcome Trust grants to F.M.G. and F.R. (WT088357/Z/09/Z and WT084210/Z/07/Z), and the Medical Research Council (Metabolic Diseases Unit, Cambridge [Ref: 4050281695] and to S.T. [Ref: MR/J013293/1]).

Duality of Interest. F.M.G. has received speaker's fees from Novo Nordisk, Merck Sharp & Dohme, and Eli Lilly; and ad hoc consulting fees from Roche and Pfizer. F.R. has received speaker's fees from Merck Sharp & Dohme and Novo Nordisk, and ad hoc consulting fees from AstraZeneca. H.E.P. received speaker's fees from Merck Sharp & Dohme. No other potential conflicts of interest relevant to this article were reported.

Author Contributions. P.R., H.E.P., A.E.A., J.M.H., S.C.C., and S.T. researched data. F.M.G. designed the study, researched data, and wrote the manuscript. F.R. designed the study, researched data, and edited the manuscript. F.M.G. and F.R. are joint guarantors of this work and, as such, had full access to all the data in the study and take responsibility for the integrity of the data and the accuracy of the data analysis.

References

1. Holst JJ. The physiology of glucagon-like peptide 1. Physiol Rev 2007;87:1409–1439
2. During MJ, Cao L, Zuzga DS, et al. Glucagon-like peptide-1 receptor is involved in learning and neuroprotection. Nat Med 2003;9:1173–1179
3. Fields AV, Patterson B, Karnik AA, Shannon RP. Glucagon-like peptide-1 and myocardial protection: more than glycemic control. Clin Cardiol 2009;32:236–243
4. Samson SL, Bajaj M. Potential of incretin-based therapies for non-alcoholic fatty liver disease. J Diabetes Complications 2013;27:401–406
5. Nachnani JS, Bulchandani DG, Nookala A, et al. Biochemical and histological effects of exendin-4 (exenatide) on the rat pancreas. Diabetologia 2010;53:153–159
6. Drucker DJ. Incretin action in the pancreas: potential promise, possible perils, and pathological pitfalls. Diabetes 2013;62:3316–3323
7. Thorens B. Expression cloning of the pancreatic beta cell receptor for the gluco-incretin hormone glucagon-like peptide 1. Proc Natl Acad Sci U S A 1992;89:8641–8645
8. Reimann F, Habib AM, Tolhurst G, Parker HE, Rogers GJ, Gribble FM. Glucose sensing in L cells: a primary cell study. Cell Metab 2008;8:532–539
9. Hansen L, Deacon CF, Orskov C, Holst JJ. Glucagon-like peptide-1-(7-36) amide is transformed to glucagon-like peptide-1-(9-36)amide by dipeptidyl peptidase IV in the capillaries supplying the L cells of the porcine intestine. Endocrinology 1999;140:5356–5363
10. Vahl TP, Tauchi M, Durler TS, et al. Glucagon-like peptide-1 (GLP-1) receptors expressed on nerve terminals in the portal vein mediate the effects of endogenous GLP-1 on glucose tolerance in rats. Endocrinology 2007;148:4965–4973
11. Li N, Lu J, Willars GB. Allosteric modulation of the activity of the glucagon-like peptide-1 (GLP-1) metabolite GLP-1 9-36 amide at the GLP-1 receptor. PLoS ONE 2012;7:e47936
12. Ban K, Noyan-Ashraf MH, Hoefer J, Bolz SS, Drucker DJ, Husain M. Cardioprotective and vasodilatory actions of glucagon-like peptide 1 receptor are mediated through both glucagon-like peptide 1 receptor-dependent and -independent pathways. Circulation 2008;117:2340–2350
13. Shimshek DR, Kim J, Hübner MR, et al. Codon-improved Cre recombinase (iCre) expression in the mouse. Genesis 2002;32:19–26
14. Luche H, Weber O, Nageswara Rao T, Blum C, Fehling HJ. Faithful activation of an extra-bright red fluorescent protein in "knock-in" Cre-reporter mice ideally suited for lineage tracing studies. Eur J Immunol 2007;37:43–53
15. De Marinis YZ, Salehi A, Ward CE, et al. GLP-1 inhibits and adrenaline stimulates glucagon release by differential modulation of N- and L-type Ca2+ channel-dependent exocytosis. Cell Metab 2010;11:543–553
16. Kim M, Platt MJ, Shibasaki T, et al. GLP-1 receptor activation and Epac2 link atrial natriuretic peptide secretion to control of blood pressure. Nat Med 2013;19:567–575
17. Merchenthaler I, Lane M, Shughrue P. Distribution of pre-pro-glucagon and glucagon-like peptide-1 receptor messenger RNAs in the rat central nervous system. J Comp Neurol 1999;403:261–280

18. Kedees MH, Guz Y, Grigoryan M, Teitelman G. Functional activity of murine intestinal mucosal cells is regulated by the glucagon-like peptide-1 receptor. Peptides 2013;48:36–44
19. Sivertsen J, Rosenmeier J, Holst JJ, Vilsbøll T. The effect of glucagon-like peptide 1 on cardiovascular risk. Nat Rev Cardiol 2012;9:209–222
20. Gardiner SM, March JE, Kemp PA, Bennett T, Baker DJ. Possible involvement of GLP-1(9-36) in the regional haemodynamic effects of GLP-1 (7-36) in conscious rats. Br J Pharmacol 2010;161:92–102
21. Moreno C, Mistry M, Roman RJ. Renal effects of glucagon-like peptide in rats. Eur J Pharmacol 2002;434:163–167
22. de Heer J, Rasmussen C, Coy DH, Holst JJ. Glucagon-like peptide-1, but not glucose-dependent insulinotropic peptide, inhibits glucagon secretion via somatostatin (receptor subtype 2) in the perfused rat pancreas. Diabetologia 2008;51:2263–2270
23. Butler AE, Campbell-Thompson M, Gurlo T, Dawson DW, Atkinson M, Butler PC. Marked expansion of exocrine and endocrine pancreas with incretin therapy in humans with increased exocrine pancreas dysplasia and the potential for glucagon-producing neuroendocrine tumors. Diabetes 2013;62:2595–2604
24. Yamamoto H, Kishi T, Lee CE, et al. Glucagon-like peptide-1-responsive catecholamine neurons in the area postrema link peripheral glucagon-like peptide-1 with central autonomic control sites. J Neurosci 2003;23:2939–2946
25. Llewellyn-Smith IJ, Reimann F, Gribble FM, Trapp S. Preproglucagon neurons project widely to autonomic control areas in the mouse brain. Neuroscience 2011;180:111–121
26. Furness JB. *The enteric nervous system*. Oxford, Blackwell Publishing, 2006
27. Jørgensen NB, Dirksen C, Bojsen-Møller KN, et al. Exaggerated glucagon-like peptide 1 response is important for improved β-cell function and glucose tolerance after Roux-en-Y gastric bypass in patients with type 2 diabetes. Diabetes 2013;62:3044–3052